

## Research Article

# Ni-Ti Shape Memory Alloy Coatings for Structural Applications: Optimization of HVOF Spraying Parameters

Carmen De Crescenzo ,<sup>1</sup> Despina Karatza,<sup>1</sup> Dino Musmarra ,<sup>1</sup> Simeone Chianese ,<sup>1</sup> Theocharis Baxevanis,<sup>2</sup> Panagiota T. Dalla,<sup>3</sup> Dimitrios A. Exarchos,<sup>3</sup> Konstantinos G. Dassios ,<sup>3</sup> and Theodore E. Matikas<sup>3</sup>

<sup>1</sup>Department of Engineering, University of Campania Luigi Vanvitelli, 81031 Aversa, Italy

<sup>2</sup>Department of Mechanical Engineering, University of Houston, Houston, TX 77204, USA

<sup>3</sup>Department of Materials Science and Engineering, University of Ioannina, Ioannina 45110, Greece

Correspondence should be addressed to Dino Musmarra; dino.musmarra@unicampania.it

Received 9 February 2018; Revised 21 April 2018; Accepted 6 May 2018; Published 28 June 2018

Academic Editor: Shuo Yin

Copyright © 2018 Carmen De Crescenzo et al. This is an open access article distributed under the Creative Commons Attribution License, which permits unrestricted use, distribution, and reproduction in any medium, provided the original work is properly cited.

This work aims at contributing to the development of a revolutionary technology based on shape memory alloy (SMA) coatings deposited on-site to large-scale metallic structural elements, which operate in extreme environmental conditions, such as steel bridges and buildings. The proposed technology will contribute to improve the integrity of metallic civil structures, to alter and control their mechanical properties by external stimuli, to contribute to the stiffness and rigidity of an elastic metallic structure, to safely withstand the expected loading conditions, and to provide corrosion protection. To prove the feasibility of the concept, investigations were carried out by depositing commercial NiTinol Ni50.8Ti (at.%) powder, onto stainless steel substrates by using high-velocity oxygen-fuel thermal spray technology. While the NiTinol has been known since decades, this intermetallic alloy, as well as no other alloy, was ever used as the SMA-coating material. Due to the influence of dynamics of spraying and the impact energy of the powder particles on the properties of thermally sprayed coatings, the effects of the main spray parameters, namely, spray distance, fuel-to-oxygen feed rate ratio, and coating thickness, on the quality and properties of the coating, in terms of hardness, adhesion, roughness, and microstructure, were investigated.

## 1. Introduction

Ni-Ti shape memory alloys are extremely interesting materials both for their ability of showing the shape memory effect (SME) and for their elevated strength and ductility [1].

An attractive Ni-Ti-based SMA is NiTinol, a nearly equiatomic intermetallics of nickel and titanium. NiTinol shape memory properties were first discovered by Buehler and Wiley at the Naval Ordnance Laboratory, Maryland, United States [2] (the name NiTinol is derived from the chemical symbol “NiTi” followed by “NOL,” the acronym for Naval Ordnance Laboratory).

In common with other SMAs, NiTinol shows two important mechanical features: shape memory effect and pseudoelasticity. The former is related to fatigue and fracture resistances of an

alloy and consists in its ability to return to its initial shape upon heating to the austenite phase (high-temperature phase having B2 cubic structure) after having been deformed in the martensite phase (low-temperature monoclinic phase) [3–5]; the latter is due to the stress-induced martensitic transformation upon loading and the subsequent strain recovery upon unloading at temperatures above the austenite temperature  $A_f$  [1, 6]. NiTinol’s ability to undergo a thermal- or stress-induced martensitic phase transformation and its recoverable strains that are much greater than those in traditional alloys, specifically between 8% and 10% [3, 7], make it the most popular shape memory alloy [3].

NiTinol offers additional advantage for the targeted application since there is a good understanding of its thermo-mechanical response and the crystallography, as well as of the

effects of changes of the transformation temperatures and the heat treatment with variations in composition.

Among the several technologies for depositing metallic coatings on metallic substrates, thermal spray high-velocity oxygen-fuel (HVOF) is one of the most versatile [8] and efficient technologies, with many multiscale features [9, 10], capacity to produce homogeneous [11] and very dense coatings [12–17] with porosity levels typically in the range 0.1–2% [13], low oxide content [11, 12], high hardness [13, 18], excellent bond strength frequently exceeding 69 MPa [11, 13, 19], and low decarburization [13, 20]. Also, the low gas temperature of particles avoids superheating during flight and preserves the nanocrystalline structure of the starting powders of the coating [21].

The HVOF thermal spray system utilizes high-pressure combustion (6–10 bars for the HVOF spray system of third generation [13]) of oxygen and gaseous fuels, such as hydrogen, propane, and propylene, or liquid fuels, such as kerosene. Combustion produces a flow of hot gas at supersonic or hypersonic velocity of approximately 2000 m/s [19, 22–24]. The flame achieves supersonic velocities in the process of expansion at the exit of the convergent-divergent nozzle with a diameter size from 8 to 9 mm [13, 22] and temperatures in the range of 2500–3200°C, depending on the type of the fuel, the fuel-to-oxygen ratio, and the combustion pressure [13, 25, 26].

Powders, with typical particle sizes of 10–63 µm [13], are axially or radially introduced into the stream of gases at the exit of the nozzle [19, 26, 27], molten or semimolten in a temperature range of 900–1800°C [28], and, passing through the gun barrel nozzle, propelled with the produced gas at a supersonic velocity [29] of 300–800 m/s toward the surface of the substrate [13, 19, 26] at typical mass flow rates in the range of 2.3–14 kg/h [25].

Molten or semimolten droplets or particles cool rapidly upon impact at a range of approximately 10<sup>5</sup> K/s, causing splat quenching and resulting in very fine submicrometric crystals [30].

The HVOF thermal spray technology has primarily been used for wear-resistant coatings; however, because HVOF produces very dense coatings, it can be used for very good corrosion-resistant coatings providing longer lifetimes than the uncoated substrate [13, 19].

As reported in other studies, the properties of HVOF coatings are dependent on spraying and coating process parameters, such as spray distance, oxygen-fuel ratio, and powder feed rate [31, 32], and on chemical and physical states of particles, such as velocity, temperature, melting degree, and oxide content [31, 32]. Spray distance acts on velocity and temperature of the in-flight particles and influences porosity, hardness of the coating [31], and oxide content of the sprayed powders [23]; powder feed rate and melting degree of powders affect the coating hardness and corrosion resistance, respectively [30, 32]; the fuel-to-oxygen mixing ratio influences the flame temperature and velocity [33] and particle velocity [21] and affects oxide content and density of coating [23]. On the basis of these findings, to obtain the best properties of the coating, it is necessary to define the optimal spraying and coating parameters.

Currently, NiTi alloys are often deposited as thin films. The deposition of NiTi thin films on steel substrates has been following two main directions: the former is the direct deposition on top of a supporting structure, such as a bulk micromachined silicon cantilever [34]; the second is their use as stand-alone thin films to become microactuators [34, 35]. NiTi thin films are also used in the field of microelectromechanical systems (MEMS) for several reasons, such as their high actuation force and displacement at low frequencies [34–38], simplification of the design, and friction-free and nonvibrating movement [37]. Due to the versatility and flexibility of NiTi thin films and their multiple degrees of freedom and compact structure, they are used in the aerospace industry, automotive applications, and the biomedical field for microgrippers and implant stents because of its excellent biocompatibility [35, 37, 39].

The development of SMA thin films on metallic substrates is very challenging for three reasons: (a) it is related to the need for controlling the SMA thin-film composition; (b) it is associated to the large mismatch of thermal expansion coefficients between the substrate and thin film [40]; and (c) it is linked to the development of future applications of thin films [41]. For these reasons, very limited work exists in the literature about the deposition of potential SMA materials on substrates, and the most of them are developed for microactuating devices.

This study presents a new class of SMA-based HVOF-prone coatings for elastic metallic structures, such as civil constructions, which would contribute to their stiffness and rigidity, withstand the expected loading conditions, improve their integrity before or during their in-service life, and offer corrosion protection. Herein, the effects of thermal spraying parameters, namely, spray distance, distance between the exit of the nozzle of the HVOF gun and substrate, fuel-to-oxygen feed rate ratio, and coating thickness on the mechanical and microstructural properties of NiTinol coatings on metallic substrates are evaluated by investigating hardness, adhesion, surface roughness, and microstructure of the specimens. The optimal values of the spraying parameters are established for thermal spraying application of NiTinol powders by means of HVOF technology.

It is worth highlighting that, while there is limited work on using NiTinol as a coating material [42], the development of such coating with the shape memory effect is a pioneering objective, which was followed before the experimental work described in the present manuscript; as a consequence, the selection of a proper technology for a powdered SMA deposition technology in large scale is another innovative purpose of the present investigation.

## 2. Materials and Methods

A commercial prealloyed NiTinol, Ni50.8Ti (at.%), powder S/BB superelastic, supplied by Memry Corporation (Connecticut, USA) was used as a starting material. As per manufacturer specifications, the powder particles occupied a particle size range of 15 to 40 µm. To demonstrate the feasibility of the concept, rectangular, common stainless steel coupons, AISI-type 316, with dimensions 100 × 25 × 1.5 mm<sup>3</sup>, were employed

TABLE 1: Spraying parameters employed in the HVOF spraying process.

Spraying parameter	Spray distance (mm)	Kerosene/oxygen feed rate ratio (l/h-l/min)	Coating thickness (mm)	Specimen
Spray distance	300	20–800	0.30	A
	350	20–800	0.30	B
	400	20–800	0.30	C
Kerosene/oxygen feed rate ratio	300	20–800	0.30	A
	300	22–860	0.30	D
	300	25–900	0.30	E
Coating thickness	300	20–800	0.15	F
	300	20–800	0.30	A
	300	20–800	0.60	G

as substrates for coating deposition. A GTV HVOF-K2 system (GTV Verschleiss-Schutz GmbH, Germany) using kerosene as the liquid fuel and argon as the powder carrier gas was employed for the deposition of SMA coatings; the processes took place at the establishment of Thermal Spray Service Ltd (Italy).

To improve the adhesion of the coating, before thermal spraying, the substrates were grit-blasted with an alumina grit using an ACB shot peening machine (ACB Sabbiatrici S.R.L., Italy) up to an average Ra roughness value of  $3\text{ }\mu\text{m}$  and cleaned using compressed air. All specimens were mounted on a horizontally rotating turntable and cooled during and after spraying with compressed air jets. A robotic manipulator was programmed to operate the torch spraying NiTinol powder at predefined distances from the substrates.

A parameter variation study was carried out in order to investigate the effect of spray distance (in the range 300–400 mm), fuel-to-oxygen feed rate ratio (in the range 20 l/h–800 l/min–25 l/h–900 l/min), and coating thickness (in the range 0.15–0.60 mm) on the characteristics of the coating. The powder feed rate and argon flow rate were kept constant at 70 g/min and 8 l/min for all depositions, respectively.

Seven sets of spray parameters were considered and are summarized in Table 1.

A Galileo Ergotest COMP 25 (LTF, Italy) hardness tester was used to measure superficial Rockwell Hardness 15 N as per the requirements in ASTM E18 [43]. This test is performed to define the NiTinol coating's ability to resist a permanent indentation or deformation when in contact with a diamond cone indenter under a load of 15 kgf [44].

The adhesion of coating was tested by tensile adhesion tests as per the recommendations in the dedicated standard test method for adhesion strength of thermal spray coatings, ASTM C633 [45]. The tests were performed on a M30K universal tensile testing machine equipped with a 50 kN load cell (JJ Lloyd, UK). Therein, tensile loads were applied on the faces of thermally sprayed cylindrical specimens adhered to the sandblasted faces of identically shaped uncoated specimens. A steel specimen of diameter of 0.9 inches (about 23 mm) and length of 38.1 mm was used as given in [45]. The specimen faces were adhered together with one-part high-density epoxy adhesive, 3 M Scotch-Weld 2214, of an ultimate tensile stress of approximately 70 MPa. Coating thickness of 0.015 inches (0.38 mm) is recommended for high porosity coatings in

order to avoid possible penetration of the resin into the voids of the sprayed porous coating; if the coating porosity is less than 2%, the thickness of 0.015 inches required by the ASTM Standard is not necessary [45, 46]. Hence, 0.25 mm thick coatings were tested.

A Polytec TMS-1200 white light interference microscope with resolution 3.65 nm (Polytec GmbH, Germany) was used for rapid, noncontact, two- and three-dimensional microtopography of the materials' surface. All samples were examined at a  $2.24 \times 1.67 \text{ mm}^2$  field of view. In terms of surface profilometry, the following parameters were investigated:

- (i)  $\text{Sq}$  ( $\mu\text{m}$ ), which represents the quadratic average roughness value, "RMS" roughness within the definition area. It is equivalent to the standard deviation for surface amplitude.
- (ii)  $\text{Sa}$  ( $\mu\text{m}$ ), which represents the arithmetic average roughness value, the average surface roughness. It expresses, as an absolute value, the difference in height of each point compared to the arithmetical mean of the surface.
- (iii)  $\text{Ssk}$  (-), which represents the skewness of height distribution:  $\text{Ssk} > 0$  means that the height distribution is skewed below the mean plane.
- (iv)  $\text{Sz}$  ( $\mu\text{m}$ ), which represents the maximum height of surface texture, the height between highest profile peak and lowest profile value within the defined area.
- (v)  $\text{Spk}$  ( $\mu\text{m}$ ), which represents the reduced peak height, roughness height of profile peaks. It indicates the mean height of peaks above the core surface.

The microstructure of coating/substrate cross sections was examined by optical microscopy (OM) while the morphology of the coatings' surfaces was assessed by scanning electron microscopy (SEM). Optical microscopy provides valuable feedback on microstructural aspects such as voids, unmelted particles, lamellae obtained from particles that have been modified chemically at spraying by reduction or oxidation, and solid inclusions at the interface between the coating and substrate [46]. This investigation was performed using Nikon Eclipse L150 optical microscope (Nikon Instruments Europe BV, Netherlands).

Scanning electron microscopy allows observing the individual lamella after a "splash" onto the substrate's surface, surfaces of as-sprayed coatings, fine-grained microstructure, fine or recrystallized structure, and porosities [46]. SEM

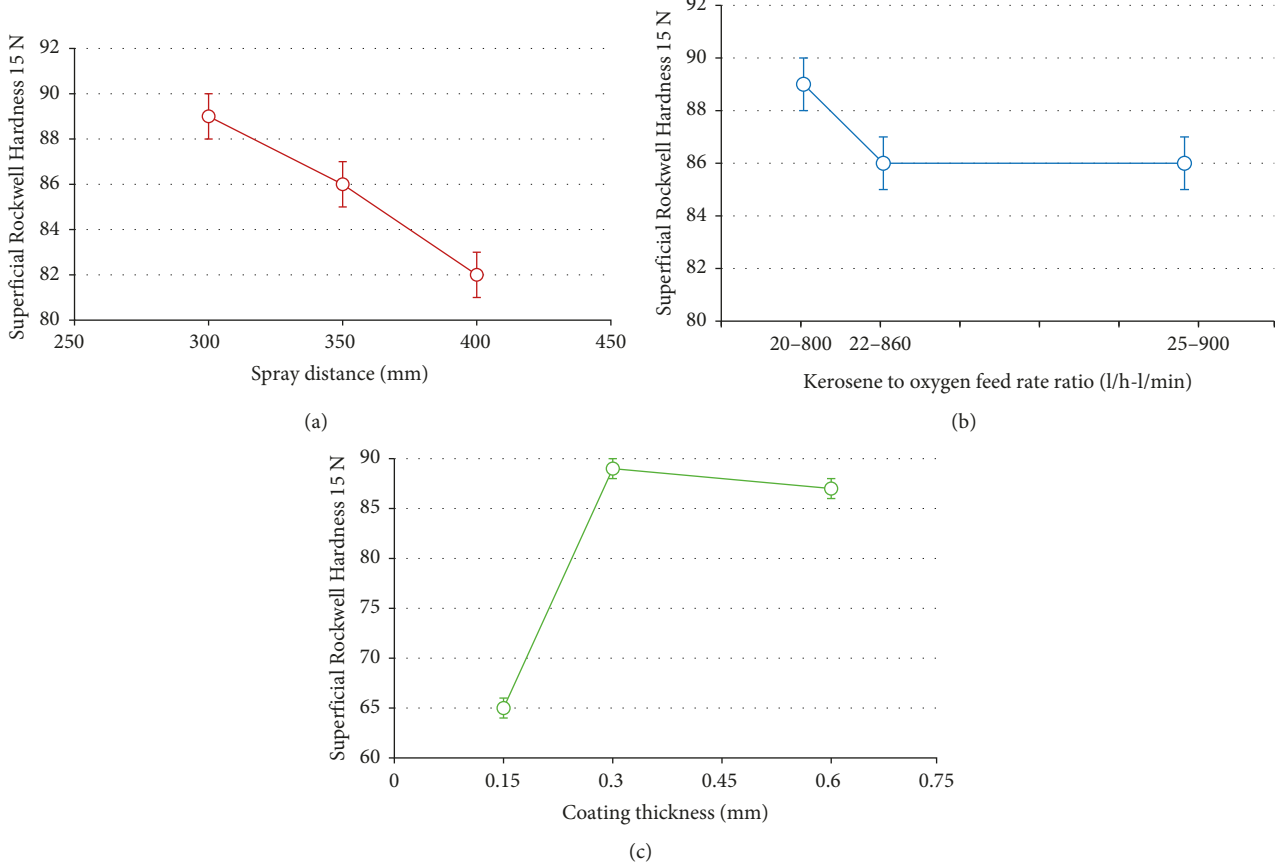


FIGURE 1: Effect of (a) spray distance, (b) kerosene to oxygen feed rate ratio, and (c) coating thickness on coating hardness.

investigations were carried out using JEOL JSM-5600 scanning electron microscope (JEOL USA, Inc., USA).

The chemical composition of the NiTinol coating was assessed using X-ray fluorescence (XRF). The XRF measurements were performed using a micro-XRF M1-Mistral X-ray fluorescence spectrometer (Bruker, Germany) with 700  $\mu\text{m}$  diameter circular beam spot.

In addition, energy dispersive spectroscopy (EDS) was used to investigate if oxidation occurred in the coating material during the deposition process by the HVOF spraying technique. The measurements were performed using an Oxford Instruments EDS system (Oxford Instruments, Oxfordshire, UK).

A TA Instruments Q series differential scanning calorimeter (DSC) (TA Instruments, New Castle, Delaware) was used to precisely determine the transformation temperatures. The temperature range of the instrument is  $-180^\circ\text{C}$  to  $600^\circ\text{C}$  while inert atmosphere was not used and cooling was performed using liquid nitrogen. The heating and cooling rates of the tests were fixed to  $10^\circ\text{C}/\text{min}$ .

### 3. Results

**3.1. Hardness of the Coating.** After grinding the specimens for equal surface roughness, the coating hardness was evaluated. The superficial Rockwell Hardness 15 N as a function of spray distance, kerosene to oxygen feed rate ratio, and coating thickness are plotted in Figure 1. The hardness increases from a value of 60, measured for the

uncoated specimen, to a minimum value of 65 with a coating thickness of 0.15 mm. Results demonstrate that Rockwell Hardness 15 N decreases monotonically by spray distance, decreases up to a plateau value with kerosene to oxygen feed rate ratio up to 22 l/h-860 l/min, whereas with coating thickness, a fluctuating behavior consisting of an initial increase up to 0.3 mm thick coating followed by a decrease thereon is noted. The maximum hardness value of 89 is attained for a spray distance of 300 mm and a kerosene to oxygen feed rate ratio of 20 l/h-800 l/min, where the coating thickness is 0.3 mm.

**3.2. Quality of Adhesion to Substrate.** In this work, the effects of spray distance and kerosene to oxygen feed rate ratio on the coating adhesion strength were studied, and the results are reported in Figure 2. It is therein observed that adhesion strength decreases with spray distance while a fluctuating behavior consisting of an initial decrease followed by increase is noted with kerosene to oxygen feed rate ratio. The maximum tensile adhesion strength corresponds to sample "E" having been thermally sprayed from a distance of 300 mm with the highest combustion energy stemming from a kerosene to oxygen feed rate ratio equal to 25 l/h-900 l/min.

**3.3. Surface Profilometry.** The arithmetic average roughness ( $\text{Sa}$ ) is the most widely used because it is a simple parameter to obtain, and it is an effective method for monitoring

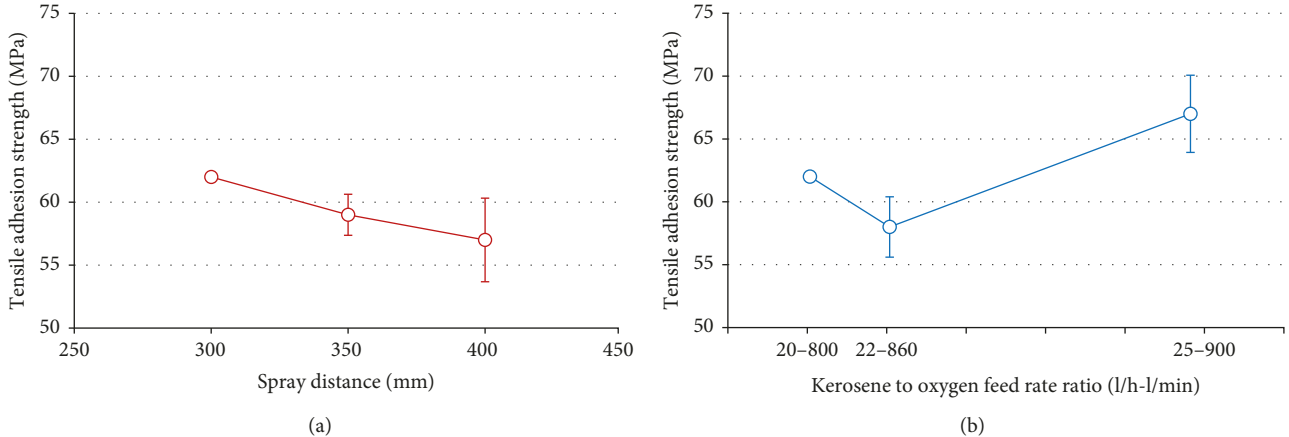


FIGURE 2: Effect of (a) spray distance and (b) kerosene to oxygen feed rate ratio on coating tensile adhesion strength.

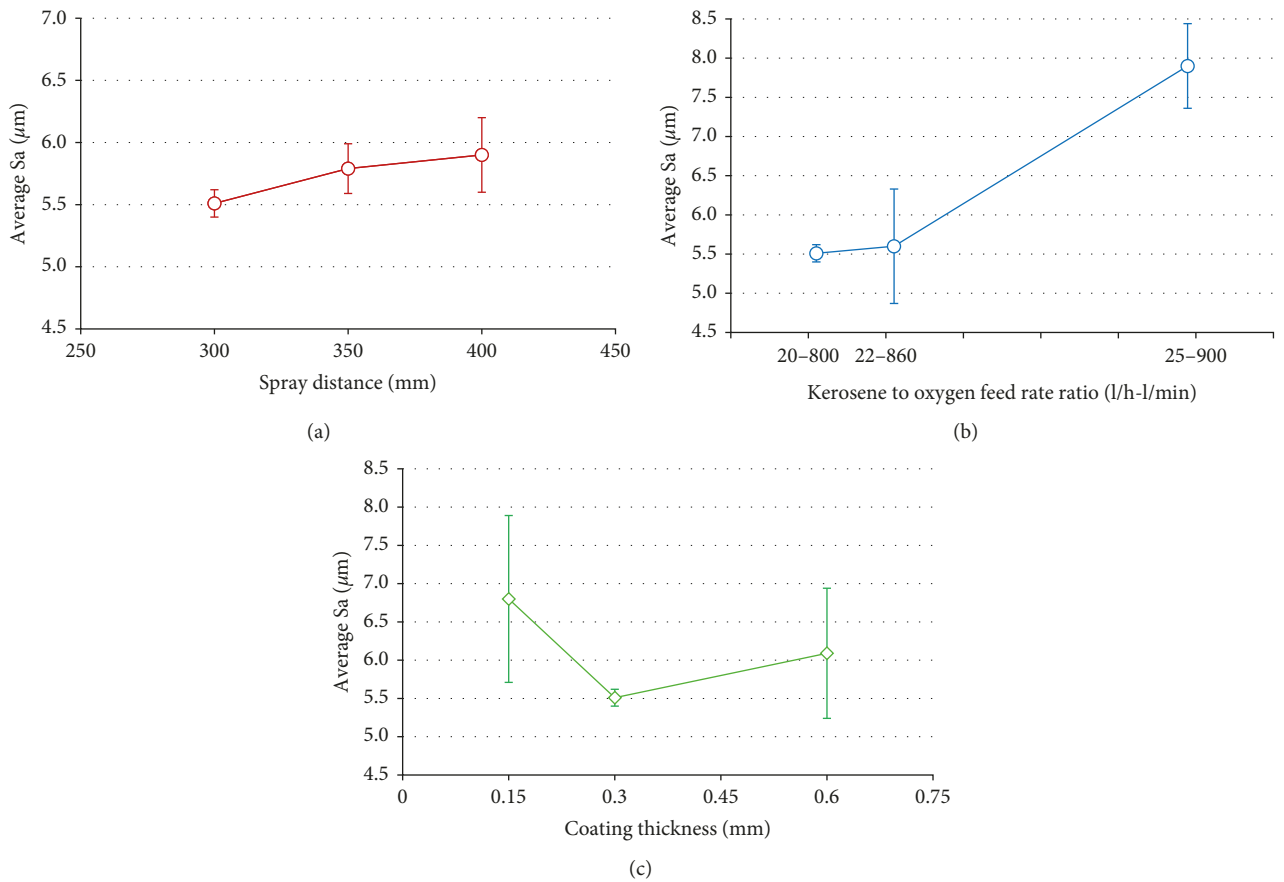


FIGURE 3: Effect of (a) spray distance, (b) kerosene to oxygen feed rate ratio, and (c) coating thickness on Sa roughness parameter.

surface texture and ensuring consistency in measurement of multiple surfaces [47].

Figure 3 depicts the variation of average Sa with spray distance, kerosene to oxygen feed rate ratio, and coating thickness.

As it can be observed in Figure 3, Sa parameter increases with spray distance and kerosene to oxygen feed rate ratio, but shows the lowest value for a coating thickness of 0.3 mm.

Specimen A shows the minimum value of roughness in terms of Sa.

The average values of the other roughness parameters investigated are reported in Table 2. Therein, it is observed that the coating of thickness of 0.30 mm on sample A, sprayed at a distance of 300 mm at a kerosene to oxygen feed rate ratio of 20 l/h-800 l/min, exhibits the optimal profilometry fingerprint with minimum values for all parameters, across all specimens.

Figure 4 illustrates the typical appearance of the morphology of NiTinol coatings' surface in two- and

TABLE 2: Surface profilometry results.

Specimen	Average Sq ( $\mu\text{m}$ )	Average Ssk	Average Sz ( $\mu\text{m}$ )	Average Spk ( $\mu\text{m}$ )
A	$6.99 \pm 0.19$	$0.31 \pm 0.13$	$92.28 \pm 17.37$	$8.00 \pm 0.62$
B	$7.38 \pm 0.05$	$0.52 \pm 0.22$	$96.44 \pm 15.7$	$9.14 \pm 1.46$
C	$7.67 \pm 0.49$	$0.37 \pm 0.05$	$115.78 \pm 10.42$	$10.09 \pm 1.23$
D	$7.21 \pm 1.01$	$0.53 \pm 0.06$	$93.72 \pm 34.68$	$9.41 \pm 1.38$
E	$10.60 \pm 1.19$	$1.10 \pm 0.64$	$102.12 \pm 8.68$	$17.59 \pm 4.86$
F	$11.31 \pm 3.74$	$0.56 \pm 0.21$	$145.13 \pm 53.98$	$19.00 \pm 8.74$
G	$7.86 \pm 1.14$	$1.32 \pm 1.47$	$104.16 \pm 43.08$	$9.40 \pm 2.17$

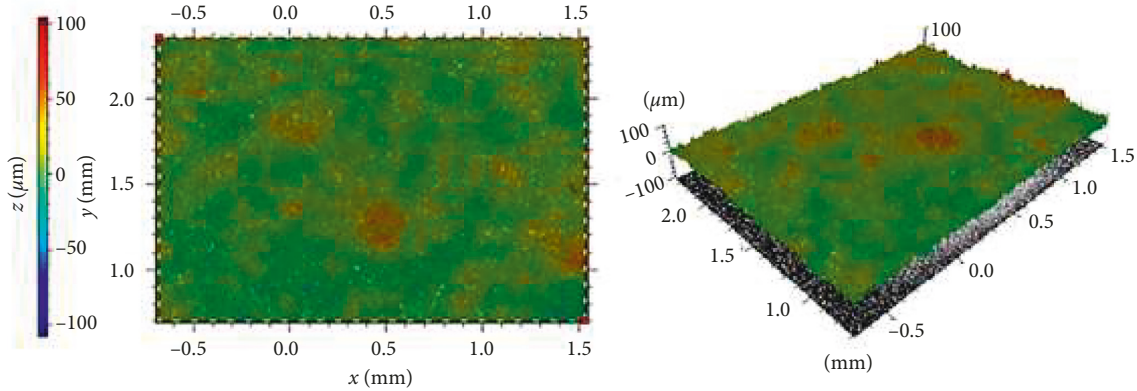


FIGURE 4: Two- and three-dimensional view of the NiTinol coating's surface observed with the light profilometer.

three-dimensional displays. Coating morphology is dependent on the different conditions of spraying process.

**3.4. Microstructure.** Scanning electron microscopy (SEM) and optical microscopy (OM) reveal good homogeneity and uniformity. All coatings present the lamellas and porous and unmelted particles that are all inherent to the HVOF thermal spraying. A better adherence is found in the coatings sprayed with the highest kerosene to oxygen ratio and lower spray distance, specimens A and E, respectively. In contrast, the highest combustion energy level may produce higher amounts of oxides attributable to the high feed rate of oxygen (E). A lower porosity is revealed in the coatings sprayed with a lower spray distance (A, D, and E) because of the shorter exposure time in flight and the high particle velocities that yield higher impact energies (Figures 5 and 6).

**3.5. Chemical Composition and Shape Memory Effect.** To assess the chemical composition of the coating material, two types of samples were used: (a) Ni-Ti-coated samples sprayed by HVOF using Ni-rich Ni50.8Ti (at.%) powder and (b) bulk SMA samples on known composition Ni50.8Ti (at.%).

Figure 7 shows the XRF results from these two types of samples that were compared for assessing the coating chemical composition. The figure clearly shows that the chemical composition of the NiTinol coating sprayed using the HVOF technique is almost identical with that of the bulk sample of known Ni50.8Ti (at.%) composition.

Figure 8(a) shows the EDS spectrum of the NiTinol coating, and Figure 8(b) depicts the corresponding EDS-layered image that gives complete picture of chemical

composition of the coating. The compositional distribution of the coating was found to be Ni50.8 (at.%) and Ti49.2 (at.%), confirming the findings of XRF. Moreover, no presence of oxygen or carbon was observed, indicating the absence of oxides or carbides in the Ni-Ti coating. This is proof that the NiTinol coating deposited on the substrate was not oxidized or burned-out during HVOF spraying.

The ability of the NiTinol SMA coating to maintain its intrinsic properties during the spraying process was assessed using differential scanning calorimetry (DSC). Ni-Ti SMAs exhibit the shape memory effect based on the thermoelastic martensitic transformation occurring during cooling and the reverse transformation occurring during heating. Hence, the DSC analysis allows assessment of the obtained shape memory effect.

The DSC curve for the NiTinol Ni50.8Ti (at.%) SMA coating is presented in Figure 9, which exhibits peaks clearly revealing transformation temperatures of  $MS = 54.2^\circ\text{C}$ ,  $Mf = 45.3^\circ\text{C}$ ,  $AS = 67.5^\circ\text{C}$ , and  $Af = 86.6^\circ\text{C}$ .

XRD measurements showed the presence of two phases in this NiTinol material, martensitic (B19') and austenitic (B2). As the cooling progresses and temperature decreases from above  $100^\circ\text{C}$  down to  $-90^\circ\text{C}$ , the intensity of B2 diffraction peak decreases, and peaks related to B19' martensite appear. On heating, the diffraction peaks corresponding to B19' start disappearing while the B2 phase peak reappears.

## 4. Discussion

The results of this study demonstrate that spray distance, kerosene to oxygen feed rate ratio, and coating thickness affect the characteristics and properties of HVOF-prone

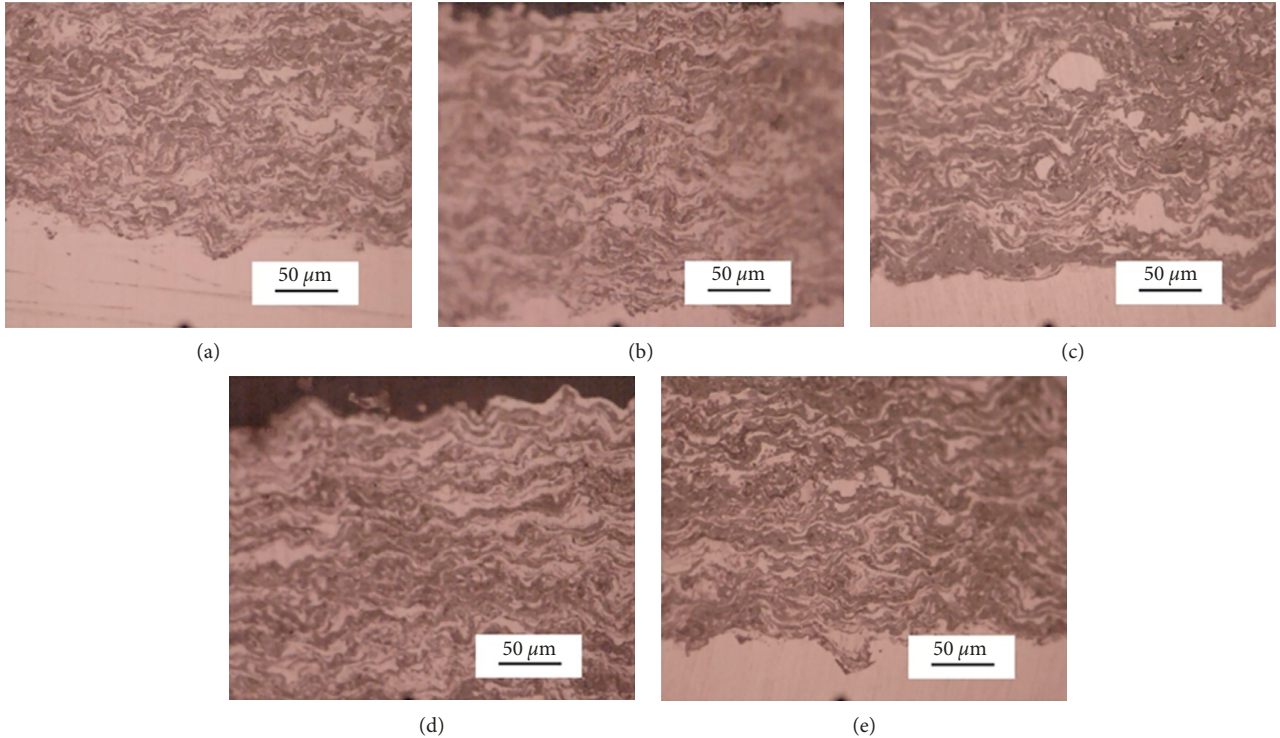


FIGURE 5: OM images of NiTinol coatings' cross section of samples A (a), B (b), C (c), D (d), and E (e).

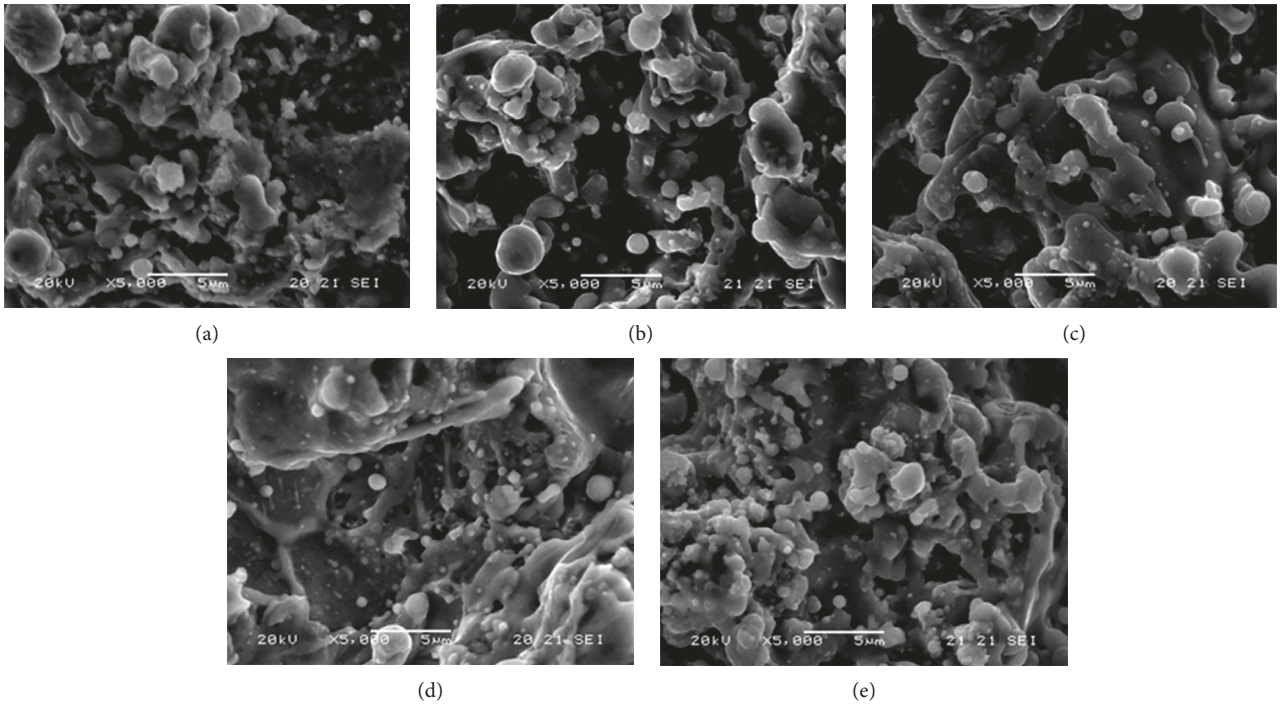


FIGURE 6: SEM micrographs of NiTinol coatings' surface of samples A (a), B (b), C (c), D (d), and E (e).

NiTinol coatings. Spray distance in particular influences both particle temperature and velocity, with higher distances found associated with increased temperatures and decreased velocities [31, 48]. Herein, the maximum values of superficial Rockwell Hardness 15 N and adhesion are achieved at

a spray distance of 300 mm, which is the lowest among distances investigated. The coatings' surface roughness is influenced by temperature and velocity of the particles [49]. At spray distance of 300 mm, surface profilometry shows lowest roughness parameters, and OM and SEM investigations

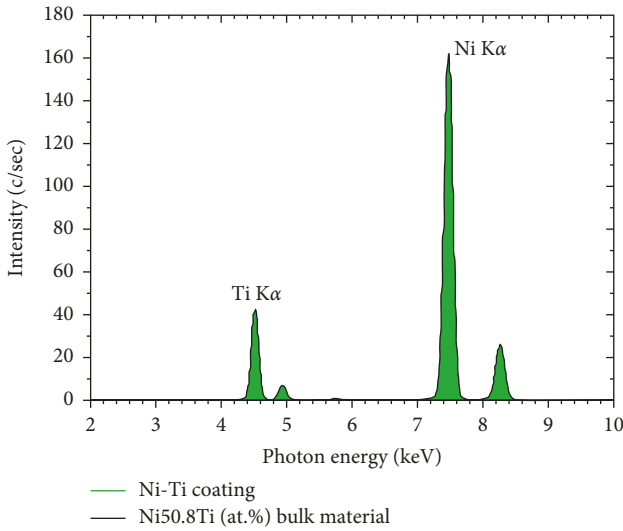


FIGURE 7: Ni and Ti K X-ray transitions from the NiTinol coating versus the bulk Ni-rich Ni50.8Ti (at.%) sample.

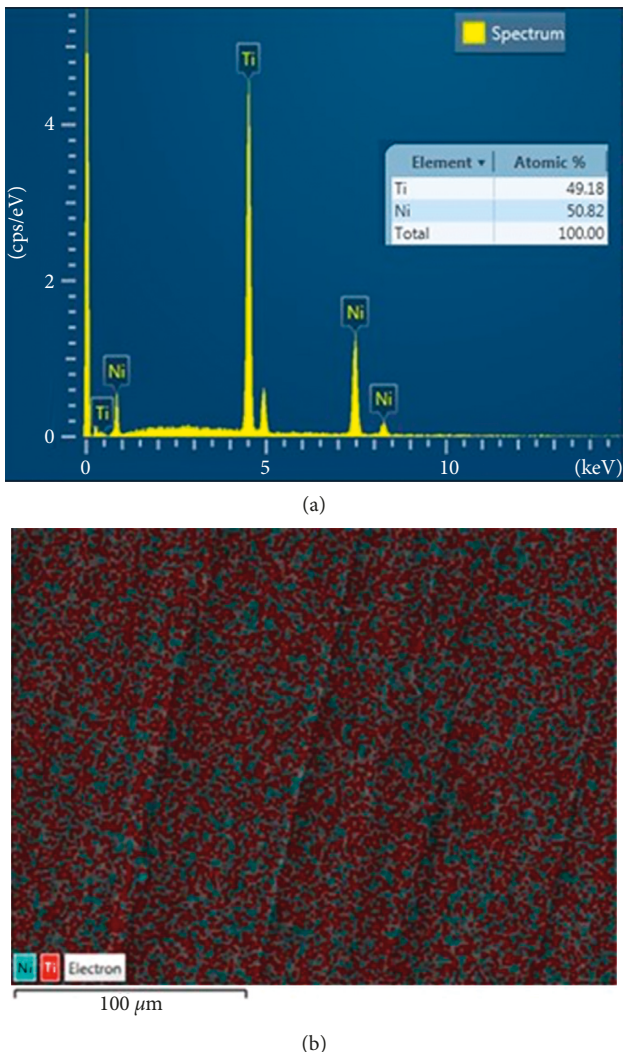


FIGURE 8: EDS results of the NiTinol coating sprayed with the HVOF technique: (a) EDS spectrum and (b) EDS-layered image.

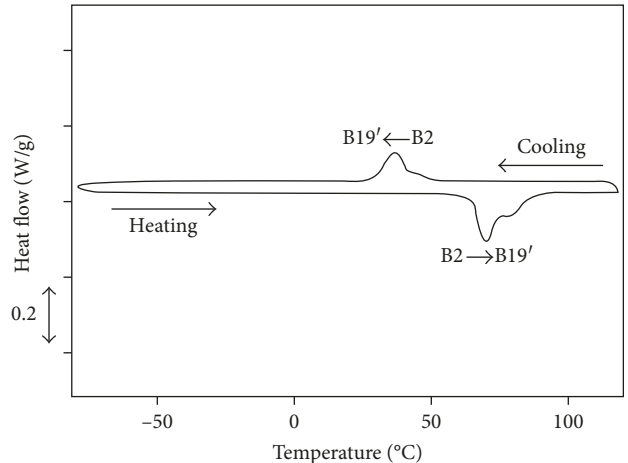


FIGURE 9: DSC curve for the NiTinol Ni50.8Ti (at.%) coating revealing its shape memory effect.

demonstrate the greatest density and lowest porosity. This behavior can be explained with the higher velocity and the higher energy of the particles that impact the substrates leading to lower porosity and higher density coatings.

The fuel to oxygen ratio influences both particle temperature and velocity: the increasing of fuel to oxygen ratio provides either a decrease in particle velocity or an increase in particle temperature [50]. Maximum hardness is obtained at kerosene to oxygen feed rate ratio of 20 l/h-800 l/min, but the highest adhesion value is observed in the coating sprayed at intermediate kerosene to oxygen feed rate ratio. The higher the kerosene to oxygen feed rate ratio, the less smooth the coatings, and OM and SEM images reveal a molten surface between substrate and coating due to the greater heat released from combustion.

XRF analysis clearly showed that the chemical composition of the NiTinol coating sprayed using the HVOF technique remained of Ni50.8Ti (at.%) composition, as the composition of the original powder used. EDS characterization also confirmed the findings of XRF. In addition, EDS showed the absence of oxides or carbides in the Ni-Ti coating, indicating that the NiTinol coating was not oxidized or burned-out during the HVOF spraying process.

Finally, the ability of the NiTinol SMA coating to maintain its intrinsic properties during the spraying process was demonstrated using DSC, which revealed the coating transformation temperatures and proved the existence of shape memory effect.

## 5. Conclusions

SMA NiTinol powder was sprayed on stainless steel AISI 316 specimens by using an industrial-scale HVOF thermal spray. The effect of spray distance, kerosene to oxygen feed rate ratio, and coating thickness on coating properties, in terms of hardness, adhesion, surface roughness, and microstructure was experimentally investigated in order to define the best set of parameters for coating application.

Best hardness was found for minimal spray distance, minimal kerosene to oxygen feed rate ratio, and for 0.3 mm

coating thickness. Coating adhesion to substrate decreased with increasing spray distance, but the highest adhesion value was observed for the coating sprayed at an intermediate kerosene to oxygen feed rate ratio. Surface profilometry revealed smoothest surfaces in the coating sprayed at shortest distance and lowest kerosene to oxygen feed rate ratio with a thickness of 0.30 mm. OM and SEM images showed greatest density in the coatings sprayed at a short distance and greater adhesion for greater kerosene to oxygen feed rate ratios.

Coating adhesion and microstructure characterization results pointed out the effectiveness of the HVOF technology for the powdered SMA-coating deposition since good adhesion conditions and good quality of the coating were achieved.

Furthermore, the optimal HVOF spraying parameter, resulting in the highest value of Rockwell Hardness 15 N (89), a great adhesion (62 MPa), lowest porosity and greatest density, and the smoothest coating surface was found for the specimen A, with a spray distance of 300 mm, a kerosene to oxygen feed rate ratio of 20 l/h-800 l/min, and a coating thickness of 0.30 mm.

Finally, it was demonstrated that the HVOF spraying technique did not alter the chemical composition of coating material in relation to the original powder and produced oxidation-free SMA coatings.

## Data Availability

The data used to support the findings of this study are available from the corresponding author upon request.

## Conflicts of Interest

The authors declare that they have no conflicts of interest.

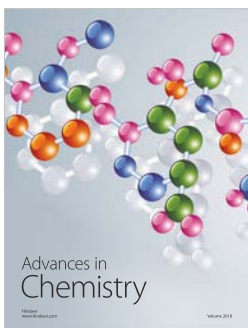
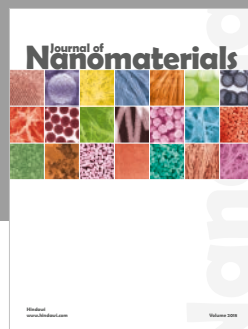
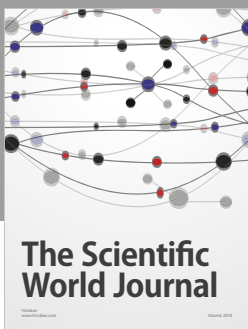
## Acknowledgments

This work has been financially supported under “Horizon 2020-The Framework Programme for Research and Innovation (2014–2020): Future and Emerging Technologies (FET Open),” project title “An Innovative Method for Improving the Structural Integrity using SMA Revolutionary Technology (InnoSMART)” (Grant agreement no. 664892). The authors would like to thank Dr. Dimitrios Anagnostopoulos and Assistant Professor Alexandros Karantzalis from the Department of Materials Science and Engineering, University of Ioannina, for assistance with the XRF and EDS measurements, respectively.

## References

- [1] K. Otsuka and X. Ren, “Physical metallurgy of Ti-Ni-based shape memory alloys,” *Progress in Materials Science*, vol. 50, no. 5, pp. 511–678, 2005.
- [2] W. Buehler and R. Wiley, *US Patent 3,174,851, Nickel-Base Alloys*, USA, 1965.
- [3] S. Robertson, A. R. Pelton, and R. O. Ritchie, “Mechanical fatigue and fracture of nitinol,” *International Materials Reviews*, vol. 57, no. 1, pp. 1–37, 2012.
- [4] L. Janke, C. Czaderski, M. Motavalli, and J. Ruth, “Applications of shape memory alloys in civil engineering structures-overview, limits and new ideas,” *Materials and Structures*, vol. 38, no. 5, pp. 578–592, 2005.
- [5] P. Novák, L. Mejzlíková, A. Michalcová, J. Čapek, P. Beran, and D. Vojtěch, “Effect of SHS conditions on microstructure of NiTi shape memory alloy,” *Intermetallics*, vol. 42, pp. 85–91, 2013.
- [6] P. Kumar and L. Dimitris, *Shape Memory Alloys: Modelling and Engineering Applications*, Springer Science Business Media, Berlin, Germany, 2008.
- [7] N. B. Morgan, “Medical shape memory alloy applications—the market and its products,” *Materials Science and Engineering*, vol. 378, no. 1-2, pp. 16–23, 2004.
- [8] V. Shibe and V. Chawla, “Combating wear of ASTM A36 steel by surface modification using thermally sprayed cermet coatings,” *Advances in Materials Science and Engineering*, vol. 2016, Article ID 3894145, 10 pages, 2016.
- [9] P. D. Christofides, N. El-Farra, M. Li, and P. Mhaskar, “Model-based control of particulate processes,” *Chemical Engineering Science*, vol. 63, no. 5, pp. 1156–1172, 2008.
- [10] M. Li and P. D. Christofides, “Modeling and control of high-velocity oxygen-fuel (HVOF) thermal spray: a tutorial review,” *Journal of Thermal Spray Technology*, vol. 18, no. 5-6, pp. 753–768, 2009.
- [11] H. Ruiz-Luna, D. Lozano-Mandujano, J. M. Alvarado-Orozco et al., “Effect of HVOF processing parameters on the properties of NiCoCrAlY coatings by design of experiments,” *Journal of Thermal Spray Technology*, vol. 23, no. 6, pp. 950–961, 2014.
- [12] T. C. Totemeier, R. N. Wright, and W. D. Swank, “FeAl and Mo-Si-B intermetallic coatings prepared by thermal spraying,” *Intermetallics*, vol. 12, no. 12, pp. 1335–1344, 2004.
- [13] T. S. Sidhu, S. Prakash, and R. D. Agrawal, “Studies on the properties of high-velocity oxy-fuel thermal spray coatings for higher temperature applications,” *Materials Science*, vol. 41, no. 6, pp. 805–823, 2005.
- [14] T. Sahraoui, S. Guessasma, M. Ali Jeridane, and M. Hadji, “HVOF sprayed WC-Co coatings: microstructure, mechanical properties and friction moment prediction,” *Materials and Design*, vol. 31, no. 3, pp. 1431–1437, 2010.
- [15] S. Hong, Y. Wu, B. Wang, Y. Zheng, W. Gao, and G. Li, “High-velocity oxygen-fuel spray parameter optimization of nanostructured WC-10Co-4Cr coatings and sliding wear behavior of the optimized coating,” *Materials and Design*, vol. 55, pp. 286–291, 2014.
- [16] M. Xie, Y. Lin, P. Ke et al., “Influence of process parameters on high velocity oxy-fuel sprayed Cr<sub>3</sub>C<sub>2</sub>-25% NiCr coatings,” *Coatings*, vol. 7, no. 7, p. 98, 2017.
- [17] E. Bakan, G. Mauer, Y. J. Sohn, D. Koch, and R. Vaßen, “Application of high-velocity oxygen-fuel (HVOF) spraying to the fabrication of Yb-silicate environmental barrier coatings,” *Coatings*, vol. 7, no. 4, p. 55, 2017.
- [18] Y. Liu, G. Gou, X. Wang, Q. Jia, H. Chen, and M. Tu, “Effects of rare earth elements on the microstructure and mechanical properties of HVOF-sprayed WC-Co coatings,” *Journal of Thermal Spray Technology*, vol. 23, no. 7, pp. 1225–1231, 2014.
- [19] J. D. Majumdar, “Thermal and cold spraying technology in manufacturing,” in *Handbook of Manufacturing Engineering and Technology*, pp. 2805–2850, Springer, Berlin, Germany, 2015.
- [20] T. Sahraoui, N. E. Fenineche, G. Montavon, and C. Coddet, “Structure and wear behaviour of HVOF sprayed Cr<sub>3</sub>C<sub>2</sub>-NiCr and WC-Co coatings,” *Materials and Design*, vol. 24, no. 5, pp. 309–313, 2003.
- [21] M. Li and P. D. Christofides, “Modeling and analysis of HVOF thermal spray process accounting for powder size distribution,” *Chemical Engineering Science*, vol. 58, no. 3–6, pp. 849–857, 2003.
- [22] D. Cheng, Q. Xu, E. J. Lavernia, and G. Trapaga, “The effect of particle size and morphology on the in-flight behavior of

- particles during high velocity oxy fuel thermal spraying," *Metallurgical and Materials Transactions B*, vol. 32, no. 3, pp. 525–535, 2001.
- [23] J. Saeedi, T. W. Coyle, H. Arabi, S. Mirdamadi, and J. Mostaghimi, "Effects of HVOF process parameters on the properties of Ni-Cr coatings," *Journal of Thermal Spray Technology*, vol. 19, no. 3, pp. 521–530, 2010.
- [24] X. Wang, Q. Song, and Z. Yu, "Numerical investigation of combustion and flow dynamics in a high velocity oxygen-fuel thermal spray gun," *Journal of Thermal Spray Technology*, vol. 25, no. 3, pp. 441–450, 2016.
- [25] S. Amin and H. Panchal, "A review on thermal spray coating processes," *International Journal of Current Trends in Engineering and Research*, vol. 2, no. 1, pp. 556–563, 2016.
- [26] L. Pawlowski, "Thermal spraying techniques," in *The Science and Engineering of Thermal Spray Coatings*, pp. 67–113, Wiley, Hoboken, NJ, USA, 2008.
- [27] P. Fauchais, J. V. Heberlein, and M. I. Boulos, "Industrial applications of thermal spraying technology," in *Thermal Spray Fundamentals*, pp. 1401–1545, Springer, Boston, MA, USA, 2014.
- [28] G. S. Settles and S. R. Bekofske, "HVOF thermal spray velocity, temperature, and stainless coating properties," in *Proceedings of the Sixteenth Symposium on Energy Engineering Sciences*, Argonne, IL, USA, May 1998.
- [29] M. Löbel, T. Lindner, T. Mehner, and T. Lampke, "Microstructure and wear resistance of AlCoCrFeNiTi high-entropy alloy coatings produced by HVOF," *Coatings*, vol. 7, no. 9, p. 144, 2017.
- [30] B. Saeedi and A. S. Rouhaghdam, "The study of high temperature oxidation behavior of different microstructures of HVOF thermally sprayed coatings," *Journal of Advanced Materials and Processing*, vol. 2, no. 2, pp. 3–12, 2014.
- [31] O. Maranho, D. Rodrigues, M. Boccalini, and A. Sinatra, "Influence of parameters of the HVOF thermal spray process on the properties of multicomponent white cast iron coatings," *Surface and Coatings Technology*, vol. 202, no. 15, pp. 3494–3500, 2008.
- [32] Y. Wang, S. L. Jiang, Y. G. Zheng et al., "Effect of processing parameters on the microstructures and corrosion behaviour of high-velocity oxy-fuel (HVOF) sprayed Fe-based amorphous metallic coatings," *Materials and Corrosion*, vol. 64, no. 9, pp. 801–810, 2013.
- [33] M. Bozorgtabar, M. Salehi, M. Rahimipour, and M. Jafarpour, "Influence of high velocity oxy-fuel parameters on properties of nanostructured TiO<sub>2</sub> coatings," *Bulletin of Materials Science*, vol. 33, no. 6, pp. 671–675, 2010.
- [34] P. Krulevitch, A. P. Lee, P. B. Ramsey, J. C. Trevino, J. Hamilton, and M. A. Northrup, "Thin film shape memory alloy microactuators," *Journal of Microelectromechanical Systems*, vol. 5, no. 4, pp. 270–282, 1996.
- [35] J. Mohd Jani, M. Leary, A. Subic, and M. A. Gibson, "A review of shape memory alloy research, applications and opportunities," *Materials and Design*, vol. 56, pp. 1078–1113, 2014.
- [36] B. Winzek, S. Schmitz, H. Rumpf et al., "Recent developments in shape memory thin film technology," *Materials Science and Engineering A*, vol. 378, no. 1-2, pp. 40–46, 2004.
- [37] Y. Fu, H. Du, W. Huang, S. Zhang, and M. Hu, "TiNi-based thin films in MEMS applications: a review," *Sensors and Actuators A: Physical*, vol. 112, no. 2-3, pp. 395–408, 2004.
- [38] S. Miyazaki and A. Ishida, "Martensitic transformation and shape memory behavior in sputter-deposited TiNi-base thin films," *Materials Science and Engineering: A*, vol. 273–275, pp. 106–133, 1999.
- [39] K. Li, X. Huang, Z. S. Zhao, Y. Li, and Y. Q. Fu, "Electrochemical and corrosion behaviors of sputtered TiNi shape memory films," *Smart Materials and Structures*, vol. 25, no. 3, p. 35039, 2016.
- [40] X. Wu, T. Pence, and D. Grummon, "Model tracking of stress and temperature induced martensitic transformations for assessing superelasticity and shape memory actuation," *MRS Proceedings*, vol. 459, 1996.
- [41] H. Kahn, W. L. Benard, M. A. Huff, and A. H. Heuer, "Titanium-nickel shape memory thin film actuators for micromachined valves," in *Proceedings of International Solid State Sensors and Actuators Conference (Transducers'97)*, pp. 227–232, Chicago, IL, USA, June 1997.
- [42] J. M. Guilemany, N. Cinca, S. Dosta, and A. V. Benedetti, "Corrosion behaviour of thermal sprayed nitinol coatings," *Corrosion Science*, vol. 51, no. 1, pp. 171–180, 2009.
- [43] ASTM E18–16, *Standard Test Methods for Rockwell Hardness of Metallic Materials*, American Society for Testing and Materials, West Conshohocken, PA, USA, 2016.
- [44] E. L. Tobolski and A. Fee, "Macroindentation hardness testing," in *ASM Handbook: Mechanical Testing and Evaluation*, pp. 428–469, ASM International, Geauga County, OH, USA, 2000.
- [45] ASTM C633–13, *Standard Test Method for Adhesion or Cohesion Strength of Thermal Spray Coatings*, American Society for Testing and Materials, West Conshohocken, PA, USA, 2017.
- [46] L. Pawlowski, "Methods of coatings' characterization," in *The Science and Engineering of Thermal Spray Coatings*, pp. 291–370, John Wiley & Sons, Ltd, 2nd edition, 2008.
- [47] G. Schuetz, *Modern Machine Shop*, 2002, <http://www.mmsonline.com/columns/surface-texture-from-ra-to-rz>.
- [48] V. V. Sobolev and J. M. Guilemany, "Investigation of coating porosity formation during high velocity oxy-fuel (HVOF) spraying," *Materials Letters*, vol. 18, no. 5-6, pp. 304–308, 1994.
- [49] Š. Houdková, M. Kašparová, and J. Schubert, "The spraying parameters optimization of the HVOF satellite 6 coating," in *Proceedings of the Metal 2012*, Brno, Czech Republic, 2012.
- [50] J. A. Hearley, J. A. Little, and A. J. Sturgeon, "The effect of spray parameters on the properties of high velocity oxy-fuel NiAl intermetallic coatings," *Surface and Coatings Technology*, vol. 123, no. 2-3, pp. 210–218, 2000.



Hindawi

Submit your manuscripts at  
[www.hindawi.com](http://www.hindawi.com)

